# An Inorganic Nanohybrid with High Specific Surface Area: $TiO_2$-Pillared $MoS_2$

Seung-Min Paek,[†] Hyun Jung,[†] Man Park,[†] Jin-Kyu Lee,[†] and Jin-Ho Choy*[,‡]

*School of Chemistry and Molecular Engineering, Seoul National University, Seoul 151-747, and Division of Nanoscience, Ewha Womans University, Seoul 120-750, Korea*

*Received December 29, 2004. Revised Manuscript Received April 25, 2005*

A novel lamellar inorganic−inorganic nanohybrid ($TiO_2$-pillared $MoS_2$) has been successfully synthesized by an exfoliation-reassembling method. According to the X-ray diffraction and cross-sectional transmission electron microscopy analyses, quantum-sized $TiO_2$ nanoparticles with a diameter of 1 nm are homogeneously distributed in the interlayer space of a two-dimensional $MoS_2$ lattice. Such structural regularity of pillars results in a remarkable enhancement of porosity, as confirmed by nitrogen adsorption−desorption isotherms. The Langmuir specific surface area (186 $m^2\ g^{-1}$) of the $TiO_2$-pillared $MoS_2$ has been determined to be remarkably larger than that (12 $m^2\ g^{-1}$) of the restacked $MoS_2$. It is, therefore, evident that adequate intercalation of $TiO_2$ nanoparticles into a $MoS_2$ lattice gives rise to a highly porous structure. Ti K-edge extended X-ray absorption fine structure (EXAFS) analyses also indicate that the anatase nanopillars are stabilized in the interlayer space of $MoS_2$ without any significant agglomeration. From Mo K-edge EXAFS studies, it has been found that the highly distorted octahedral structure of the host lattice in the as-prepared nanohybrid changes into a thermodynamically stable trigonal prismatic one upon heat treatment.

## Introduction

Molybdenum disulfide ($MoS_2$) with a layered structure has been extensively investigated in recent years. Of particular interest, $MoS_2$ has been known as a sulfur removal catalyst of heterocyclic organic molecules such as thiophene and dibenzothiophene,[1] as a photocatalyst and solar cell material due to its narrow indirect band gap of ∼1.2 eV, which gives rise not only to its visible-light-harvesting function but also to its high stability against photocorrosion,[2] and as a cathode material for rechargeable lithium batteries.[3]

For all these applications, it has been highly required to develop a new route to porous $MoS_2$ with high specific surface area. Especially when utilized as a catalyst in a hydrodesulfurization process and/or photocatalysis, the porosity may exert a significant effect on the accessibility of the target molecules to catalytically active sites. From this viewpoint, intense research interest has focused on the synthesis of $MoS_2$-based porous frameworks, such as solvothermally prepared nanostructured $MoS_2$[4] and porous $MoS_2$ made from ammonium thiomolybdate by thermal decomposition.[5] In addition, various synthetic approaches result in the highly dispersed $MoS_2$ with high surface area.[6−9] As a reliable alternative to porous layered materials, however, a pillaring reaction has been suggested as the most effective method of soft chemical fabrication of a new porous framework with a controlled pore structure.[10,11] In general, 2-dimensional pillared solids can be formed by the intercalation of polymeric inorganic cations in the interlayer region of layered solids. After calcination, the precursor cations transform into nanoclusters of the corresponding metal oxide which force the layers permanently apart. The presence of inorganic pillars strongly interacting with the layers gives rise to thermally stable materials with high surface area and pore volume valid for catalysis.

Recently, we were quite successful in preparing a $TiO_2$-pillared layered titanate with high porosity and enhanced photocatalytic activity via an exfoliation-reassembling route.[12] Such a pillaring strategy can be extended to the fabrication of $MoS_2$-based porous compounds. When the layered $MoS_2$ can be readily exfoliated into single sheets in an appropriate solution to form a colloid, the resulting colloidal nanosheets in suspension can be reassembled in the presence of proper pillaring agents in the solution.[13,14] To date, a number of cluster

* To whom correspondence should be addressed. Phone: +82-2-3277-4135. Fax: +82-2-3277-4340. E-mail: jhchoy@ewha.ac.kr.
† Seoul National University.
‡ Ewha Womans University.

(1) Grange, P. *Catal Rev.*—Sci. Eng. **1980**, *21*, 135.
(2) Wilcoxon, J. P. *J. Phys. Chem. B* **2000**, *104*, 7334.
(3) Tributsch, H. *Faraday Discuss. Chem. Soc.* **1980**, *70*, 190.
(4) Berntsen, N.; Gutjahr, T.; Loeffler, L.; Gomm, J. R.; Seshadri, R.; Tremel, W. *Chem. Mater.* **2003**, *15*, 4498.
(5) Leist, A.; Stauf, S.; Löken, S.; Finckh, E. W.; Lüdtke, S.; Unger, K. K.; Assenmacher, W.; Mader, W.; Tremel, W. *J. Mater. Chem.* **1998**, *8*, 241.
(6) Bezhverkhy, I.; Afanasiev, P.; Lacroix, M. *Inorg. Chem.* **2000**, *39*, 5416.
(7) Alonso, G.; Berhault, G.; Paraguay, F.; Rivera, E.; Fuentes, S.; Chianelli, R. *Mater. Res. Bull.* **2003**, *38*, 1045.
(8) Alonso, G.; Valle, M.; Cruz, J.; Petranovskii, V.; Licea-Claverie, A.; Fuentes, S. *Catal. Today* **1998**, *43*, 117.
(9) Li, W.; Shi, E.; Ko, J.; Chen, Z.; Ogino, H.; Fukuda, T. *J. Cryst. Growth* **2003**, *250*, 418.
(10) Corma, A. *Chem. Rev.* **1997**, *97*, 2373.
(11) Choy, J. H.; Park, J. H.; Yoon, J. B. *J. Phys. Chem. B* **1998**, *102*, 5991.
(12) Choy, J. H.; Lee, H. C.; Jung, H.; Kim, H.; Boo, H. *Chem. Mater.* **2002**, *14*, 2486.
(13) Joensen, P.; Frindt, R. F.; Morrison, S. R. *Mater. Res. Bull.* **1986**, *21*, 457.

10.1021/cm0477220 CCC: $30.25 
Published on Web 05/20/2005

particles or metal complexes have been hybridized with the $MoS_2$ sheets by the reassembling technique to form microporous pillared $MoS_2$ compounds. However, all the efforts so far seem to have been unsuccessful in enhancing the specific surface area and the thermal stability[15−17] due to the structural instability of the interlayer pillars, since they would have to experience a drastic structural transition from monomeric species to oligomeric ones in the process of heat treatment. To overcome such a problem, the titanium dioxide nanoparticle was selected as a pillaring agent to prop open the layers of $MoS_2$ because of its high thermal and structural stability.

In this study, we have attempted to reassemble exfoliated $MoS_2$ nanosheets in the presence of anatase sol particles to create a new porous $TiO_2$-pillared $MoS_2$ as the first example of a porous oxide−chalcogenide nanohybrid system. Along with structural characteristics, the local structure around molybdenum and the role of the $TiO_2$ pillars in enhancing the porosity are fully investigated by EXAFS spectroscopy that can probe the structural evolution upon pillaring reaction.[18,19]

## Experimental Section

**Sample Preparation.** $TiO_2$-pillared $MoS_2$ nanohybrid (hereafter abbreviated as TMN) was synthesized by the exfoliation-reassembling technique. The host molybdenum sulfide (2H−$MoS_2$), was lithiated by a 3-fold molar excess of 1.6 M *n*-BuLi for 3 days to prepare $LiMoS_2$. The product $LiMoS_2$ was washed with *n*-hexane in a glovebox and dried in a vacuum. Subsequently, deionized and degassed water was added to $LiMoS_2$ to produce a suspension of exfoliated $MoS_2$ in a concentration of 1 g/L, and the suspension was sonicated for 10 min.[13] Monodisperse nanosol particles of $TiO_2$ with a size of 1 nm were prepared by the hydrolysis of titanium butoxide in the presence of acetylacetone and *p*-toluenesulfonic acid.[20] The aqueous suspension of exfoliated $MoS_2$ was mixed with the ethanolic solution of $TiO_2$ nanosol (10:1 molar ratio of Ti to Mo). After the mixture was stirred for 24 h, the flocculated product was centrifuged, washed several times with distilled water and ethanol (1:1, v/v), and dried in a vacuum. Finally, as-prepared sample (hereafter abbreviated as TMN-rt) was heated at 150 and 300 °C for 1 h under an argon atmosphere to produce the intercalation-type nanohybrids (hereafter abbreviated as TMN150 and TMN300, respectively).

**Sample Characterization.** All the X-ray diffraction patterns were obtained with a powder X-ray diffractometer (Philips PWD 3810) using graphite-monochromated Ni-filtered Cu Kα radiation ($\lambda = 1.5418$ Å). For the HRTEM study, the TMNs were embedded into acrylic resin (methyl methacrylate:*n*-butyl methaacrylate = 4:6, benzoyl peroxide 1.5%) in a polyethylene capsule. The embedded nanohybrids were ultramicrotomed into thin slices with a diamond knife. The HRTEM study was carried out with a Philips CM200 at an accelerating voltage of 200 kV. Elemental analysis was carried out using inductively coupled plasma (ICP) spectrometry (Shimazu ICPS-5000) and a CE-Instruments-EA-1110 CHNO-S analyzer. To trace the thermal behavior of TMNs, thermogravimetric analysis (TGA) was carried out with a Rigaku TAS-100 at a heating rate of 5 °C $min^{-1}$. According to the elemental analysis from ICP spectrometry, CHNS analysis, and TGA, the chemical formula of TMN-rt was determined as $(TiO_2)_{0.32}(acetylacetone)_{0.06}MoS_2 \cdot 0.3H_2O$. The variation in particle morphology was monitored by a scanning electron microscope (Hitachi S-4300) operating at an accelerating voltage of 30 kV. Nitrogen adsorption−desorption experiments were perfomed volumetrically at liquid nitrogen temperature (78 K), as previously described.[19] The calcined samples were degassed at 150 °C for 1 h under vacuum prior to the adsorption measurements.

**X-ray Absorption Measurement.** The X-ray absorption spectroscopy (XAS) experiments at the Ti K-edge and Mo K-edge were performed with the extended X-ray absorption fine structure (EXAFS) facility installed at beamlines 7C and 10B in the Photon Factory, Tsukuba, and partly at beamline 7C in the Pohang Accelerator Laboratory, Korea. All the samples were ground to a fine powder and diluted with BN in a mortar to form a homogeneous mixture which was then packed into a 0.5 mm thick cell with Kapton tape. The XAS data were collected at room temperature in a transmission mode using Ar/He gas-ionization detectors. All the present spectra were calibrated by measuring the spectra of Mo or Ti metal foil simultaneously with those of the samples. The data analyses were carried out by the standard procedure as described previously.[21] In the case of Ti K-edge EXAFS spectra, to avoid damping of the spectra, three scans per sample were averaged out, and then the resulting EXAFS spectra were analyzed. Briefly, for the EXAFS data analyses, the inherent background in the data was removed by fitting a polynomial to the preedge region and extrapolating it through the entire spectrum, from which it was subtracted. We employed the UWXAFS 2.0 code for EXAFS analyses.[22] In the course of the nonlinear least-squares curve fitting between the experimental spectrum and a theoretical one calculated by the ab initio FEFF 6.0 code, structural parameters such as the coordination number (CN), bond distance ($R$), Debye−Waller factor ($\sigma^2$), and threshold energy difference ($\Delta E$) were optimized as variables.[23] The amplitude reduction factors were obtained from the reference compounds.

## Results and Discussion

Figure 1 represents the powder X-ray diffraction (XRD) patterns for the pillared nanohybrids and pristine $MoS_2$, and the latter (Figure 1a) has space group $P6_3/mmc$ with cell parameters of $a = 0.3160$ nm and $c = 1.2295$ nm.[24] TMN-rt (Figure 1b) shows a series of well-defined (00$l$) reflections, which indicate a highly ordered lamellar structure along the crystallographic *c*-axis. This remarkable layer expansion after the reassembling reaction clearly demonstrates that $TiO_2$ nanosol particles are intercalated into the interlayer spaces of the $MoS_2$ lattice. The mean diameter of $TiO_2$ nanoparticles has been previously reported to be about 1 nm with a narrow size distribution.[20] The interlayer distance (1.03 nm) of TMN-rt, determined by subtracting the thickness (0.62 nm) of the

(14) Divigalpitiya, W. M. R.; Frindt, R. F.; Morrison, S. R. *Science* **1989**, *246*, 369.
(15) Bissessur, R.; Heising, J.; Hirpo, W.; Kanatzidis, M. G. *Chem. Mater.* **1996**, *8*, 318.
(16) Dungey, K. E.; Curtis, M. D.; Penner-Hahn, J. E. *Chem. Mater.* **1998**, *10*, 2152.
(17) Heising, J.; Bonhomme, F.; Kanatzidis, M. G. *J. Solid State Chem.* **1998**, *139*, 22.
(18) Choy, J. H.; Yoon, J. B.; Jung, H.; Park, J. H. *J. Mater. Chem.* **2003**, *13*, 557.
(19) Choy, J. H.; Jung, H.; Han, Y. S.; Yoon, J. B.; Shul, Y. G.; Kim, H. J. *Chem. Mater.* **2002**, *14*, 3823.
(20) Scolan, E.; Sanchez, C. *Chem. Mater.* **1998**, *10*, 3217.
(21) Teo, B. K. *EXAFS: Basic Principles and Data Analysis*; Springer-Verlag: Berlin, 1986.
(22) Stern, E. A.; Newville, M.; Ravel, B.; Yacoby, Y.; Haskel, D. *Physica B* **1995**, *208* and *209*, 117.
(23) Rehr, J. J.; Zabinsky, S. I.; Albers, R. C. *Phys. Rev. Lett.* **1992**, *69*, 3397.
(24) Wyckoff, R. W. G. *Crystal Structures*; Wiley-Interscience: New York, 1965.

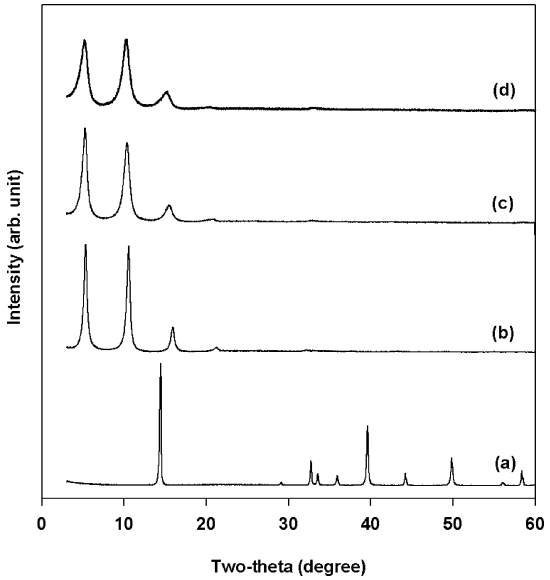


**Figure 1.** XRD patterns for (a) pristine $MoS_2$, (b) TMN-rt, (c) TMN150, and (d) TMN300.

$MoS_2$ layer from the basal spacing (1.65 nm), is in good agreement with the average size (ca. 1 nm) of $TiO_2$ nanoparticles, suggesting that a monolayer of $TiO_2$ nanoparticles is formed in the intersheet region. Generally, the interlayer distance of $TiO_2$-pillared layered materials becomes shorter upon heating due to the dehydration of solvent molecules and/or the dehydroxylation of $TiO_2$ nanosol particles in the interlayer space.[12] In the case of TMN150, however, its basal spacing of 1.70 nm was determined to be larger than that of TMN-rt. A similar result was also observed by drying the sample in a vacuum for 24 h. Such an unusual basal expansion (0.05 nm) after heat or vacuum treatments could be attributed to an increase in the coordination number of $TiO_2$ pillars, which will be discussed in detail in the EXAFS section. According to a structural study carried out on $TiO_2$ nanoparticles of different sizes, some oxygen vacancies on the surface could exist due to their very small particle size.[25] These vacant sites give rise to coordinately unsaturated titaniums in the $TiO_2$ pillars where the water molecules are ligated in the interlayer space of the nanohybrid. Similar phenomena have also been found in crystalline anatase particles under mild heating conditions at 150 °C.[26,27] TMN300 shows a basal spacing identical to that of TMN150. Though the consecutive heat treatments result in a slight broadening of (00*l*) reflections, the $TiO_2-MoS_2$ hybrid maintains its lamellar structure up to 350 °C, but collapsed to the $2H-MoS_2$ phase beyond 400 °C.[16]

Scanning electron microscopy (SEM) images of $MoS_2$ and TMN-rt are illustrated in Figure 2. It is apparent that TMN-rt forms a continuous and relatively homogeneous matrix with clear lamella morphology. It is evident that the incorporation of $TiO_2$ nanoparticles into $MoS_2$ sheets leads to the morphological changes in the cleavage along the crystallographic *c*-axis in agreement with the results of XRD

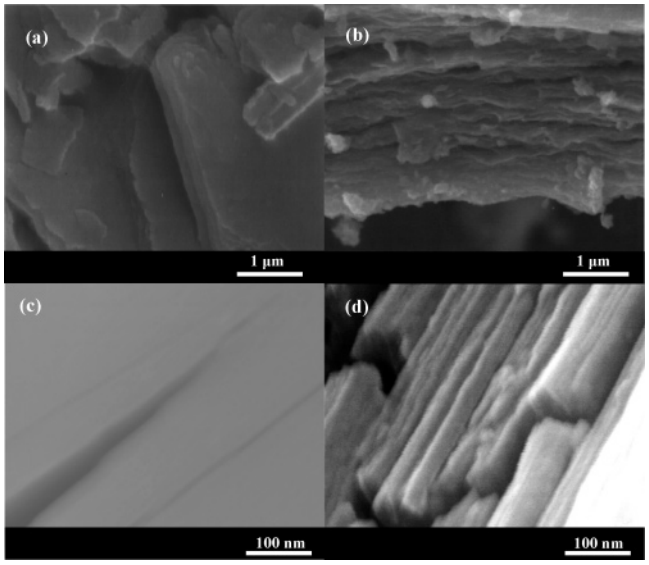


**Figure 2.** SEM images of (a) pristine $MoS_2$ with low magnification, (b) TMN-rt with low magnification, (c) pristine $MoS_2$ with high magnification, and (d) TMN-rt with high magnification.

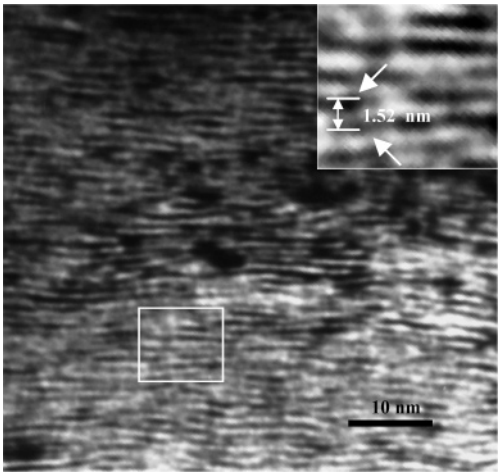


**Figure 3.** Cross-sectional HRTEM image of TMN-rt. The inset shows a magnified HRTEM image. The white arrows indicate the scattering centers corresponding to $TiO_2$ pillars.

patterns, but these can be seen only at high resolution. More significantly, the SEM micrographs also suggest that there is no bulk deposition of $TiO_2$ particles on the surface of microcrystallites.

Clear evidence of such an unusual pillared structure was directly obtained from the high-resolution transmission electron microscopy (HRTEM) image of cross-sectioned $TiO_2$-pillared $MoS_2$ nanohybrid. As shown in Figure 3, the *ab*-planes are oriented parallel to the optical axis of the microscope, where the well-developed parallel black stripes can be attributed to the layered framework of molybdenum disulfide and the delocalized spots are due to the $TiO_2$ nanoparticles in the nanohybrid. A highly oriented structure along the *c*-axis, as confirmed by the XRD study, reveals that a fine textural manipulation of the nanohybrid is successfully achieved in the reassembling process. The basal spacing of $TiO_2$-pillared $MoS_2$ was estimated to be $1.52 \pm 0.15$ nm, which is very consistent with that estimated from the XRD analysis.

To check the thermal stability of TMN-rt, TGA was carried out. As shown in Figure 4, the TGA curve can be divided

(25) Chen, L. X.; Rajh, T.; Wang, Z.; Thurnauer, M. C. *J. Phys. Chem. B* **1997**, *101*, 10688.
(26) Primet, M.; Pichat, P.; Mathieu, M.-V. *J. Phys. Chem.* **1971**, *75*, 1216.
(27) Primet, M.; Pichat, P.; Mathieu, M.-V. *J. Phys. Chem.* **1971**, *75*, 1221.

**Table 1. Parameters Obtained from $N_2$ Adsorption−Desorption Measurements**

| sample | thermal treatment (°C) | specific surface area $S_{BET}$ ($m^2\ g^{-1}$) | specific surface area $S_{Langmuir}$ ($m^2\ g^{-1}$) | slit width[a] (Å) | $V_t$[b] (mL $g^{-1}$) | $V_{micro}$[c] (mL $g^{-1}$) |
|---|---|---|---|---|---|---|
| TMN150 | 150 | 147 | 186 | 8.0 | 0.104 | 0.062 |
| TMN300 | 300 | 78 | 86 | 14.0 | 0.092 | 0.045 |
| restacked $MoS_2$ | | 6 | 12 | | 0.017 | |

[a] From a *t*-plot. [b] $V_t$ = total pore volume. [c] $V_{micro}$ = micropore volume.

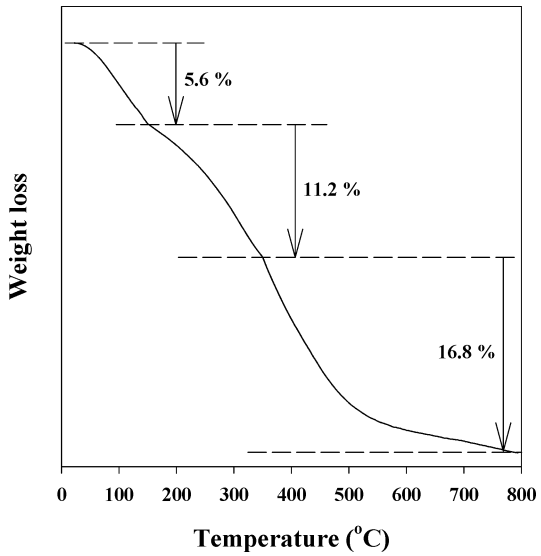


**Figure 4.** TGA curves for TMN-rt.

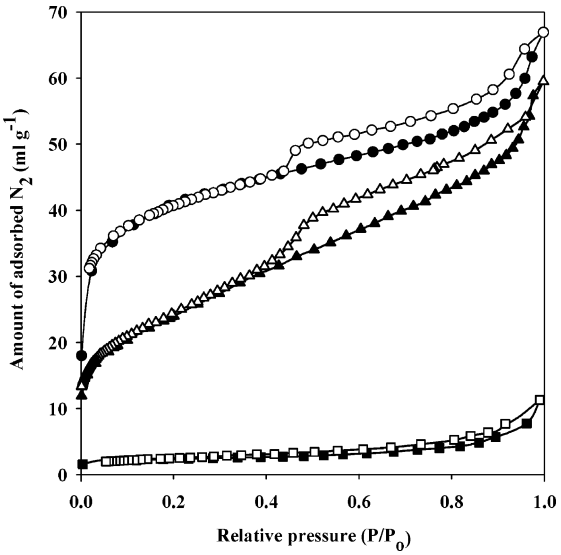


**Figure 5.** $N_2$ adsorption−desorption isotherms for the restacked $MoS_2$ (squares), TMN150 (circles), and TMN300 (triangles).

into three domains of 25−150, 150−350, and 350−600 °C, where the first mass change corresponds to the removal of hydrated $H_2O$ molecules and acetylacetone, the second one to the dehydroxylation of $TiO_2$ nanoparticles,[12] and the third one to the collapse of pillars along with the phase transformation of the host $MoS_2$ into $MoO_3$. It is, therefore, desirable to carry out the pillaring reaction in the temperature domain of 150−350 °C, in which the stability of the samples is guaranteed.

Since the pillar structure could result in a remarkable enhancement of microporosity, $N_2$ adsorption−desorption isotherm analyses have been carried out for pillared nanohybrids together with restacked $MoS_2$, as shown in Figure 5, and the parameters are summarized in Table 1. The adsorption isotherm for restacked $MoS_2$ can be assigned as type III, which is characteristic of nonporous or macroporous solids, according to the BDDT (Brunauer, Deming, Deming, and Teller) classification. However, the isotherm for TMN150 can be classified as a type between I and IV, which is indicative of the coexistence of micro- and mesopores.[28] The characteristic shape of type I at a lower relative pressure is due to the interlayer cavities produced by the pillaring reaction,[29] but the hysteresis loop resembles type B in Boer's five types, resulting from slit-shaped pores between parallel layers.[30] Furthermore, the narrow hysteresis loop indicates that the pores in TMN150 are quite open. The isotherm and hysteresis loop of TMN300 were also found to be very similar to those of TMN150, indicating that the present nanohybrids are highly porous due to the pillared structure.

As shown in Table 1, the surface area and total pore volume of TMN150 and TMN300 are greatly increased upon pillaring of $TiO_2$ nanoparticles into layered $MoS_2$. Since the adsorption isotherm of TMN150 gives a better fit to the Langmuir equation than the BET one, it can be considered that the monolayer nitrogen adsorption takes place due to the restricted pore dimensions. The Langmuir specific surface area ($S_{Langmuir}$) of TMN150 has been determined to be 186 $m^2\ g^{-1}$, which is surprisingly larger than those of the restacked $MoS_2$ (12 $m^2\ g^{-1}$) and the other pillared chalcogenides (10−80 $m^2\ g^{-1}$).[15,17,31,32] To the best of our knowledge, such a value (186 $m^2\ g^{-1}$) is the largest among transition-metal oxide- and chalcogenide-pillared $MoS_2$ compounds up to now. In the case of TMN300, it shows a fairly large Langmuir specific surface area of 86 $m^2\ g^{-1}$, suggesting that the microporous pillared structure is maintained up to 300 °C.

To evaluate the microporosity of TMN150 and TMN300, a *t*-plot analysis was carried out using the adsorption branch, as shown in Figure 6, where the adsorbed nitrogen content is plotted against the statistical thickness (*t*), obtained from a standard *t*-curve of the Harkins−Jura equation.[30] The micropore volume ($V_{micro}$) is estimated using the line extrapolated from the high-pressure branch to the adsorption axis, and the slit width is determined by doubling the *t*-value of the inflection point, which deviates downward from the

(28) Gregg, S. J.; Sing, K. S. W. *Absorption, Surface Area and Porosity*; Academic Press: London, 1982.
(29) Kooli, F.; Sasaki, T.; Watanabe, M. *Langmuir* **1999**, *15*, 1090.
(30) Allen, T. *Particle Size Measurement*, 4th ed.; Chapman and Hall: London, 1980.
(31) Heising, J.; Kanatzidis, M. G. *J. Am. Chem. Soc.* **1999**, *121*, 11720.
(32) Lee, J. K.; Lee, W.; Yoon, T. J.; Park, G. S.; Choy, J. H. *J. Mater. Chem.* **2002**, *12*, 614.

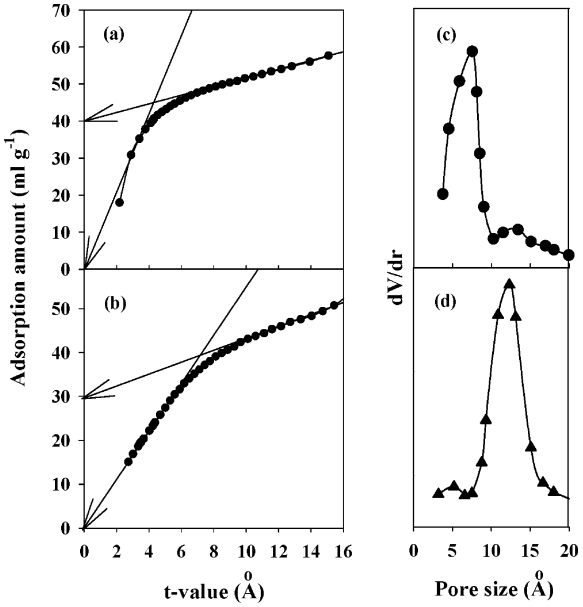


**Figure 6.** *t*-plots calculated from $N_2$ adsorption−desorption isotherms (left) for (a) TMN150 and (b) TMN300 and the pore size distribution curves (right) for (c) TMN150 and (d) TMN300.

high-pressure branch. If the sample is a nonporous solid, a straight line should pass through or close to the origin. However, the *t*-curves show horizontal and vertical departures, which indicate the presence of micropores. The slit widths of TMN150 and TMN300 are estimated to be about 0.8 and 1.4 nm, respectively, as summarized in Table 1. The inflection point in the *t*-plot of TMN150 shows a smooth variation in the range 0.3−0.5 nm, corresponding to a slit width of 0.6−1.0 nm. In the *t*-plot for TMN300, the inflection point is in the range 0.5−0.9 nm, showing a slight increase of the slit width upon heating. The micropore volumes for TMN150 and TMN300 are estimated as 0.062 and 0.045 mL $g^{-1}$, respectively, and the micropore constitutes a major part of the total porosity in both samples. In the pore size distribution curves (Figure 6c,d) calculated from the micropore analysis (MP method), TMN150 shows a slit width of about 0.8 nm, and the pore size of TMN300 is in the range 1.0−1.6 nm. It is, therefore, concluded again that the homogeneous distribution of $TiO_2$ pillars results in the formation of micropores in the interlayer space of layered molybdenum disulfide. This is surely due to the nonaggregated $TiO_2$ nanoparticles chelated by acetylacetone ligands that maintain their structures unchanged even after the hybridization with $MoS_2$, as indicated in the TEM image.[12]

One more important factor affecting the porosity of the pillared $MoS_2$ is thought to be the content of the pillaring agent. From the elemental analysis, the chemical formula of TMN150 was determined to be $(TiO_2)_{0.32}MoS_2$. Provided that spherical $TiO_2$ nanoparticles (with 13 atoms of titanium) with a diameter of 1 nm were intercalated into molybdenum disulfide in the manner of a close-packed monolayer, the maximum molar ratio of the intercalated $TiO_2$ could be calculated as approximately 0.75 per molybdenum atom. The loading of $TiO_2$ in this pillared nanohybrid was determined to be only half of the theoretical loading capacity, indicating that quite a lot of void spaces are formed in this pillared nanohybrid.

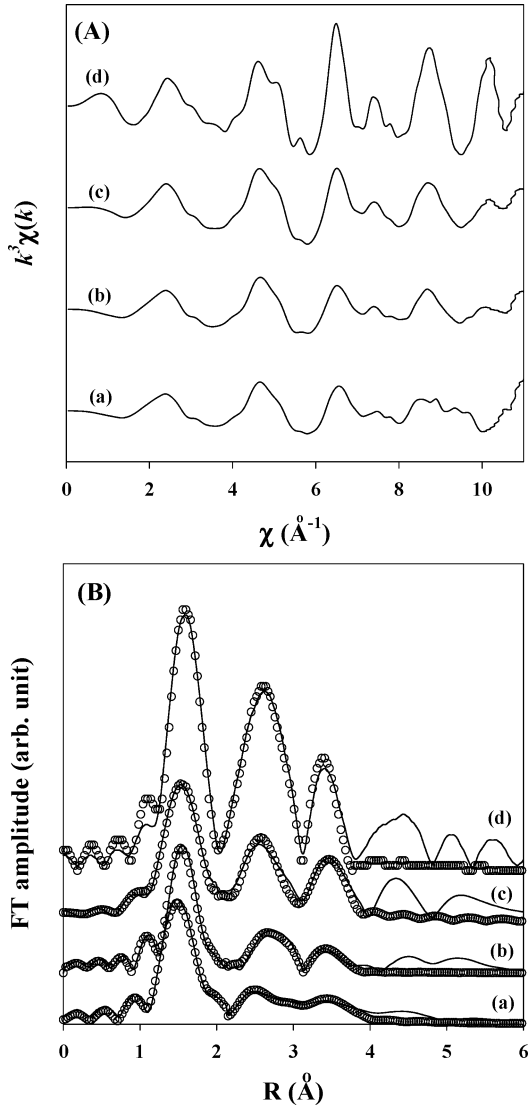


**Figure 7.** (A) $k^3$-weighted Ti K-edge EXAFS spectra for (a) TMN-rt, (b) TMN150, (c) TMN300, and (d) anatase $TiO_2$. (B) Fourier transforms (solid lines) and fitting results (circles) for (a) TMN-rt, (b) TMN150, (c) TMN300, and (d) anatase $TiO_2$.

To investigate the local structure and stability of the $TiO_2$ pillars in TMNs, the Ti K-edge $k^3$-weighted EXAFS spectra and their Fourier transforms (FTs) for TMN-rt, TMN150, and TMN300, together with anatase as a reference compound, were examined as shown in Figure 7. The spectral features of TMNs are found to be similar to that of the bulk anatase, but the oscillation amplitude (Figure 7A) becomes larger due to the fact that the crystallinity improves as the calcination temperature increases. The peaks at 1.5, 2.5, and 3.5 Å in FTs (non-phase-shift-corrected) can be assigned to the contribution of Ti−O, edge-shared Ti−Ti, and corner-shared Ti−Ti, respectively. To obtain further structural information, a nonlinear least-squares curve fitting was carried out in the range $R \leq 4$ Å. The three single scattering paths Ti−O, Ti−$Ti_{edge}$, and Ti−$Ti_{corner}$ were chosen in the final fitting procedure, and the coordination numbers were normalized to those of the crystalline anatase. The fitting results and the best-fit parameters are summarized in Table 2.

According to the Ti K-edge EXAFS results, the bond distance for the first shell (Ti−O) in the crystalline anatase

**Table 2. Results of Nonlinear Least-Squares Curve-Fitting Analysis for the Ti K-Edge EXAFS Spectra of $TiO_2$-Pillared $MoS_2$ Nanohybrids[a]**

| compound | bond | CN[b] | $R^b$ (Å) | $\Delta E^b$ (eV) | $\sigma^{2\,b}$ (Å$^2$) |
|---|---|---|---|---|---|
| anatase (reference) | Ti−O | 6.0 | 1.96 | | |
| | Ti−Ti | 4.0 | 3.04 | | |
| | Ti−Ti | 4.0 | 3.79 | | |
| TMN-rt | Ti−O | 0.8 | 1.86 | | 0.004 |
| | Ti−O | 4.0 | 2.01 | −2.41 | 0.006 |
| | Ti−Ti | 2.3 | 3.11 | | 0.006 |
| | Ti−Ti | 2.3 | 3.73 | | 0.005 |
| TMN150 | Ti−O | 1.0 | 1.86 | | 0.002 |
| | Ti−O | 4.5 | 2.00 | −0.27 | 0.003 |
| | Ti−Ti | 3.0 | 3.11 | | 0.005 |
| | Ti−Ti | 3.0 | 3.70 | | 0.004 |
| TMN300 | Ti−O | 5.9 | 1.96 | | 0.001 |
| | Ti−Ti | 3.7 | 3.05 | −2.42 | 0.005 |
| | Ti−Ti | 3.8 | 3.77 | | 0.003 |

[a] The fitting range for $k$ is 2.7−10.1 Å$^{-1}$, and that for $R$ is 0.6−4.0 Å. [b] Errors in CN (coordination number) and $\sigma^2$ (Debye−Waller factor) are 20%, and those in $R$ (interatomic distance) and $\Delta E$ (threshold energy difference) are 0.02 Å and 1.8 eV, respectively.

**Table 3. Results of Nonlinear Least-Squares Curve-Fitting Analysis for the Mo K-edge EXAFS Spectra of $TiO_2$-pillared $MoS_2$ Nanohybrids[a]**

| compound | bond | CN[b] | $R^b$ (Å) | $\Delta E^b$ (eV) | $\sigma^{2\,b}$ (Å$^2$) |
|---|---|---|---|---|---|
| $MoS_2$ (reference) | Mo−S | 6.0 | 2.41 | | |
| | Mo−Mo | 6.0 | 3.15 | | |
| | Mo−S | 4.6 | 2.42 | | 0.004 |
| restacked $MoS_2$ | Mo−Mo | 0.8 | 2.77 | −3.15 | 0.005 |
| | Mo−Mo | 0.9 | 3.25 | | 0.005 |
| | Mo−Mo | 1.3 | 3.80 | | 0.002 |
| | Mo−S | 5.5 | 2.42 | | 0.003 |
| TMN-rt | Mo−Mo | 1.2 | 2.78 | −1.72 | 0.005 |
| | Mo−Mo | 1.4 | 3.27 | | 0.005 |
| | Mo−Mo | 1.6 | 3.78 | | 0.004 |
| TMN150 | Mo−S | 5.6 | 2.41 | −1.39 | 0.003 |
| | Mo−Mo | 3.5 | 3.16 | | 0.003 |
| TMN300 | Mo−S | 5.8 | 2.41 | −0.30 | 0.003 |
| | Mo−Mo | 4.2 | 3.18 | | 0.003 |

[a] The fitting range for $k$ is 2.1−12.5 Å$^{-1}$, and that for $R$ is 0.6−4.0 Å. [b] Errors in CN (coordination number) and $\sigma^2$ (Debye−Waller factor) are 20%, and those in $R$ (interatomic distance) and $\Delta E$ (threshold energy difference) are 0.02 Å and 1.8 eV, respectively.

was determined to be 1.96 Å. However, the EXAFS spectra for TMN-rt and TMN150 could not be fitted with the same single Ti−O shell; instead a two-shell model, with a shorter distance of 1.85 Å and a longer distance of 2.00 Å, provides a reasonable fit. It was, therefore, necessary to introduce the second Ti−O distance in the EXAFS curve fittings of TMN-rt and TMN150, considering the Ti−OH with a shorter bond distance on the surface of anatase nanoparticles.[34,35] It is worth noting here that the numbers of oxygen and titanium neighbors in TMN-rt and TMN150 are rather small compared to those in bulk anatase. Nearly all the $TiO_6$ octahedra in a 1 nm $TiO_2$ nanoparticle are exposed on the external surface, and consequently, they have higher surface curvature and less continuous surfaces, resulting in smaller neighboring atoms. In addition, as expected from the XRD analysis, TMN150 has a higher coordination number for the first oxygen shell than that of TMN-rt. It is, therefore, plausible that water molecules in the pillared nanohybrid migrate into the vacant oxygen sites in the $TiO_2$ pillar after mild thermal treatment at 150 °C. On the other hand, the Ti−O bond distance of 1.96 Å in TMN300 is similar to that in anatase. However, the FT peaks of the second and third shells in TMN300, corresponding to edge- and corner-shared Ti, have been determined to be significantly smaller in comparison to those of the crystalline anatase. The coordination numbers for the second and third shells in TMN300 are also found to be smaller than those of anatase, which confirms that the $TiO_2$ pillars in TMN300 are still nanosized. In addition, the depression of FT peaks in TMNs is probably due to the destructive interference of Ti atoms with neighboring Mo atoms in the layered lattices, which suggests that $TiO_2$ nanoparticles are pillared in the interlayer spaces of $MoS_2$. The other noticeable feature is that the FT peaks at 4−6 Å originated from the multiple scattering paths with focusing effects are nearly suppressed in the pillared nanohybrids, in contrast to the very crystalline $TiO_2$, indicating the nanocrystalline nature of $TiO_2$ pillars in the present hybrids.

The local structural variation of the host $MoS_2$ upon exfoliation and reassembling has also been examined in detail using the Mo K-edge EXAFS spectroscopy. The $k^3$-weighted Mo K-edge EXAFS spectra for TMNs, restacked $MoS_2$, and pristine $MoS_2$ are represented in Figure 8A with their corresponding FTs in Figure 8B. As shown in Figure 8A, the overall feature of the EXAFS spectrum of TMN-rt is quite similar to that of restacked $MoS_2$, indicating an analogous local structure around molybdenum in both samples. On the other hand, the EXAFS spectra of TMN150 and TMN300 are virtually identical to that of pristine $MoS_2$. In addition, complex oscillation patterns around $k = 4-6$ Å$^{-1}$ and $k = 10-12$ Å$^{-1}$, observed in EXAFS spectra for pristine $MoS_2$, are also present in the spectra for TMN150 and TMN300, which suggests that both of them are very similar to pristine $MoS_2$ in terms of local structure around the Mo atom.

Before EXAFS fitting, a closer inspection of the FTs of TMNs was made. In the FT diagrams (Figure 8B), the pristine 2H−$MoS_2$ has two peaks around 1.9 and 2.9 Å (non-phase-shift-corrected) corresponding to the Mo−S and Mo−Mo shells, respectively. On the other hand, the restacked $MoS_2$ exhibits four FT peaks at ∼1.9, ∼2.4, ∼2.8, and ∼3.4 Å (non-phase-shift-corrected), which can be attributed to a Mo−S shell and three kinds of Mo−Mo shells in a distorted $MoS_6$ octahedron, respectively. Upon carrying out the exfoliation-reassembling reaction, the FT peaks of restacked $MoS_2$ become depressed in comparison to those of pristine $MoS_2$ because the well-known symmetry change from the trigonal prismatic to the distorted octahedral coordination around molybdenum gives rise to a structural disorder, resulting in a damping of the EXAFS signal. TMN-rt also exhibits depressed FT peaks with four shells similar to those of the restacked $MoS_2$. From this observation, it would be expected that the Mo atoms in TMN-rt are octahedrally distorted, but upon heat treatment, TMN-rt gradually reverts to the 2H−$MoS_2$ phase as shown in Figure 8B. The FT spectral features of TMN150 and TMN300 are similar to

(33) Morand, R.; Lopez, C.; Koudelka-Hep, M.; Kedzierzawski, P.; Augustynski, J. *J. Phys. Chem. B* **2002**, *106*, 7218.
(34) Chen, L. X.; Rajh, T.; Wang, Z.; Thurnauer, M. C. *J. Phys. Chem. B* **1997**, *101*, 10688.
(35) Hanley, T. L.; Luca, V.; Pickering, I.; Howe, R. F. *J. Phys. Chem. B* **2002**, *106*, 1153.

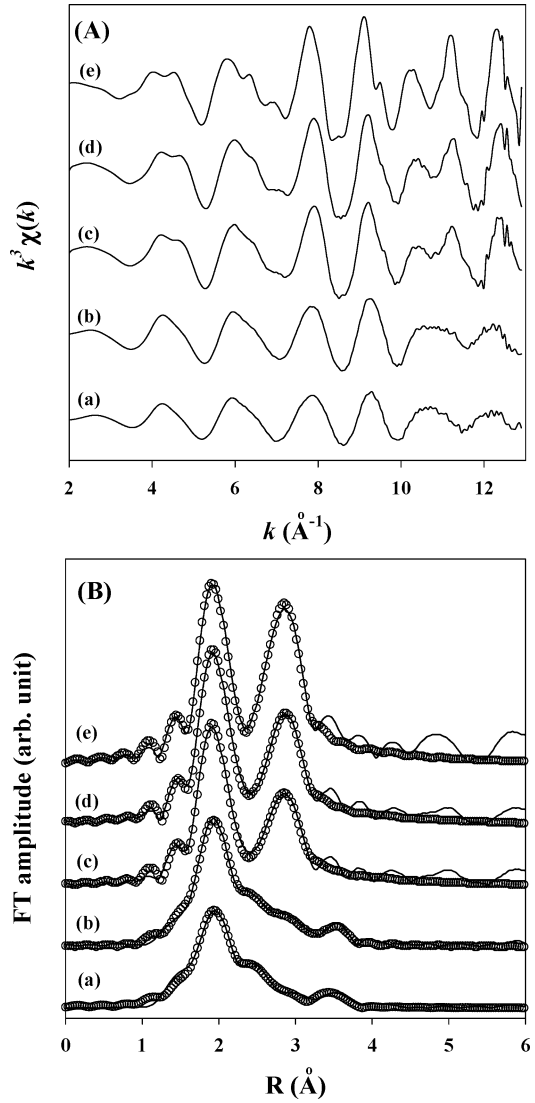


**Figure 8.** (A) $k^3$-weighted Mo K-edge EXAFS spectra for (a) restacked $MoS_2$, (b) TMN-rt, (c) TMN150, (d) TMN300, and (e) pristine $MoS_2$. (B) Fourier transforms (solid lines) and fitting results (circles) for (a) restacked $MoS_2$, (b) TMN-rt, (c) TMN150, (d) TMN300, and (e) pristine $MoS_2$.

that of pristine 2H−$MoS_2$.

The FT peaks were curve-fitted in the range $R \leq 4$ Å, and structural parameters such as the coordination number, bond distance, and Debye−Waller factor were determined. For the fitting of experimental FTs of TMNs, previously reported models, including those of 2H−$MoS_2$, $LiMoS_2$, and $Ag_xMoS_2$, were used.[36,37] At first, an attempt was made to fit TMN-rt on the basis of the crystal structure of $LiMoS_2$, but there was a failure to obtain reasonable structural data. Our EXAFS fitting results show that the molybdenum framework in TMN-rt is fairly similar to that in $Ag_xMoS_2$, which is consistent with previously reported results based on atomic pair distribution function analysis.[37] This is due to the fact that the Mo atoms in $LiMoS_2$ are trivalent whereas those in TMN-rt are in the mixed-valence state of $Mo^{3+}$ and $Mo^{4+}$ after reassembling with positively charged $TiO_2$ nanoparticles. The curve fitting for TMN-rt yields three Mo−Mo bond distances of 2.78, 3.27, and 3.78 Å, reflecting that the layered framework of TMN-rt is made of highly distorted $MoS_6$ octahedra and zigzag Mo−Mo chains. The coordination number of the first shell (Mo−S) in TMN-rt was estimated to be around 6, but those of the second and third neighboring Mo atoms were determined to be somewhat smaller, indicating that the nanocrystalline nature of TMN-rt led to an incomplete coordination and/or slight departure from the ideal position upon the exfoliation and pillaring process. In the case of TMN150 and TMN300, the model based on the 2H−$MoS_2$ structure was found to be appropriate in reproducing the basic features of the experimental FTs. The average bond distances Mo−S and Mo−Mo of TMN150 and TMN300 are found to be similar to those of 2H−$MoS_2$, indicating that molybdenum atoms in TMN150 and TMN300 are stabilized in trigonal prismatic sites. Since the $MoS_2$ phase with a trigonal prismatic structure is thermodynamically more stable than that with a distorted octahedral one, the $MoS_2$ layers in the hybrids also transform into a more stable structure upon heating. It is worth noting here that the coordination number of the second shell is estimated to be 3.5 for TMN150 and 4.2 for TMN300, respectively. This implies that TMN150 and TMN300 still have some nanocrystalline nature upon pillaring in comparison with the precursor 2H−$MoS_2$. From these Mo K-edge EXAFS results, it can be concluded that the highly distorted $MoS_6$ octahedra of TMN-rt tend to transform into thermodynamically stable trigonal prismatic ones upon heat treatment.

## Conclusion

In the present study, we have demonstrated, through the exfoliation-reassembling route, how to manipulate two different inorganic materials into a novel nanohybrid system. The present $TiO_2$-pillared $MoS_2$ nanohybrid is found to be highly porous with a specific surface area of 186 $m^2\ g^{-1}$. From the EXAFS analyses we also found that nanosized $TiO_2$ pillars having an anatase structure are stabilized in the interlayer spaces of $MoS_2$, and that the highly distorted $MoS_6$ ochahedra in the as-prepared nanohybrid transform into trigonal prismatic ones upon heat treatment. The present highly microporous and semiconducting system is expected to be an excellent hybrid catalyst to harvest synergetically both UV light and visible light, and also to apply to the hydrodesulfurization process, whose catalytic performance is now under study.

**Acknowledgment.** This work was supported by the National Research Laboratory (NRL '99) and Korean Research Foundation Grant KRF-2004-041-C00187. We thank the Ministry of Education for the Brain Korea 21 fellowship.

CM0477220

(36) Petkov, V.; Billinge, S. J. L.; Larson, P.; Mahanti, S. D.; Vogt, T.; Rangan, K. K.; Kanatzidis, M. G. *Phys. Rev. B* **2002**, *65*, 092105.
(37) Hwang, S. J.; Petkov, V.; Rangan, K. K.; Shastri, S.; Kanatzidis, M. G. *J. Phys. Chem. B* **2002**, *106*, 12453.